

Line-by-line imaging of laser-produced plasmas using one-dimensional coherent four-wave mixing

D. A. Akimov,¹ A. B. Fedotov,¹ N. I. Koroteev,^{1†} R. B. Miles,² A. N. Naumov,¹
D. A. Sidorov-Biryukov¹ and A. M. Zheltikov^{1*}

¹ International Laser Center, Faculty of Physics, Moscow State University, Moscow 119899, Russia

² Department of Mechanical and Aerospace Engineering, Princeton University, Princeton, New Jersey 08544-5263, USA

An experimental technique based on coherent one-dimensional four-wave mixing (FWM) with hyper-Raman resonances was developed for line-by-line imaging of the atomic distribution of excited atoms in a low-temperature plasma of optical breakdown. Comparison of the measured time dependences of FWM intensity and plasma transmission with the results of numerical simulations of plasma expansion allows the assessment of the influence of phase mismatch and one-photon absorption on FWM in a laser-produced plasma and demonstrates that FWM images of atomic spatial distributions free of distortions due to phase mismatch and absorption can be obtained for certain stages of plasma expansion. Copyright © 2000 John Wiley & Sons, Ltd.

INTRODUCTION

Until recently, a laser-produced plasma has not been a conventional object for diagnostics by coherent four-wave mixing (FWM) spectroscopy,^{1–3} although it has been known for a long time⁴ that the cubic susceptibility of excited atoms and ions in a laser-produced plasma may be high enough to allow the generation of reliably detectable signals. At the same time, a low-temperature laser-produced plasma (with an electron temperature of several electronvolts and an electron density from 10^{16} to 10^{19} cm⁻³) proved to offer much promise as a non-linear optical medium for laser frequency up-conversion.^{5–8} Along with frequency-conversion optimization, development of the methods of laser plasma diagnostics would be important for many applications, including the investigation of ablation processes⁹ and different aspects of the interaction of laser radiation with solid targets, laser-assisted film deposition,¹⁰ element analysis, etc.

The main problems encountered in four-wave mixing (FWM) probing of laser-produced plasmas stem from intense plasma emission, a high non-resonant coherent background and strong absorption and considerable phase-mismatch effects at certain stages of plasma expansion.^{11,12} However, the main factors that drastically lower the accuracy of non-linear optical measurements in laser-produced plasmas are associated with inevitable fluctuations of plasma parameters from pulse to pulse and

the complexity of FWM spectra, featuring a tremendous number of lines that are difficult to interpret and that often mask the spectral lines of interest. Luckily, coherent four-photon spectroscopy provides us with a rich variety of tools to solve the problems listed above. In particular, the level of incoherent background can be considerably decreased by means of time gating and spatial filtering of the FWM signal,¹³ while the coherent background can be suppressed with an appropriate choice of the polarization vectors of the pumping and probing fields, as well as the orientation of the polarization analyzer.^{3,12} Another polarization technique, often referred to as holographic multi-dimensional spectroscopy (a review of numerous Lorentzian line applications of this technique was given elsewhere¹⁴) also provides an opportunity to resolve closely spaced and overlapping lines related to different plasma species and to investigate these lines independently of each other, eventually improving the sensitivity of four-photon spectroscopy.¹⁵

Fluctuation of parameters is the problem inherent in the diagnostics of laser-produced plasmas. Since each laser pulse, in fact, creates a new plasma, any averaging procedure gives rise to considerable experimental errors^{11,16} and lowers the usefulness of laser diagnostics, especially in the case when fast processes in spatially inhomogeneous plasmas have to be investigated. A radical solution to this problem lies in the application of folded FWM schemes in broad beams, which can provide information on the spatial distribution of species from a certain area rather than from a single point of the plasma. Applying such multi-point FWM schemes to the investigation of a laser-produced plasma, we can extract information concerning 3-D spatial distributions of atoms and ions in the plasma line by line or even slice by slice.

The idea of using broad-beam coherent FWM to image a whole field of parameters of a gas medium rather than to obtain information from a single point is not new. As

* Correspondence to: A. M. Zheltikov, International Laser Center, Faculty of Physics, Moscow State University, Moscow 119899, Russia; e-mail: zheltikov@nls1.ilc.msu.ru

† Deceased.

Contract/grant sponsor: US Civilian Research and Development Foundation for the Independent States of the Former Soviet Union (CRDF); Contract/grant number: RP1-255.

Contract/grant sponsor: INTAS; Contract/grant number: 97-0369.

early as 1973, Regnier and Taran¹⁷ discussed the possibility of implementing a photographic detection of the anti-Stokes signal with a plane-wave geometry of light beams in coherent anti-Stokes Raman scattering (CARS).^{1–3,18,19} Murphy *et al.*²⁰ successfully applied one-dimensional vibrational CARS with large-angle phase matching to the investigation of a CH₄ jet. Single-pulse spatially and spectrally resolved broadband rotational multi-point CARS along a line in a gas flow with the use of a large-angle folded geometry was implemented by Snow *et al.*²¹ Several convenient and elegant schemes of two-dimensional (2-D) imaging have been recently developed with the use of degenerate four-wave mixing (DFWM),²² a technique that was initially employed for phase conjugation²³ and that later proved to be an efficient spectroscopic technique.²⁴ Ewart and co-workers observed and investigated DFWM involving excited states of Na atoms^{25,26} and developed the DFWM technique for point-by-point mapping of the distribution of Na atoms in a flame.²⁷ Subsequent studies in this direction demonstrated the possibility of applying coherent FWM in broad beams for single-pulse 2-D imaging and mapping of spatial distributions of species^{28,29} in gas media. A comprehensive analysis of many methodological problems of DFWM imaging, including diffraction effects, spatial resolution, and image referencing, has been provided by Ewart *et al.*³⁰ Results presented by Jonuscheit *et al.*³¹ suggest that, with a proper arrangement of focusing and collimating optics, CARS can also provide an efficient means for single-pulse one-dimensional temperature measurements. Recently, the first application of the folded coherent four-wave mixing technique based on hyper-Raman resonances for imaging lead atoms in a laser-produced plasma was demonstrated.³²

In this paper, the possibility of non-linear optical imaging of atoms in laser-produced plasmas with the use of folded hyper-Raman resonant FWM mixing in broad beams is demonstrated. We investigate the main factors influencing the intensity of coherent FWM in laser-produced plasmas with allowance for one-photon absorption and phase matching and present a model of plasma kinetics. We also describe the experimental technique and the methods of measurements employed for the FWM probing of laser-produced plasmas. The results of our measurements are discussed and analyzed in terms of characteristic parameters of coherent FWM in laser-produced plasmas.

HYPER-RAMAN RESONANT FOUR-WAVE MIXING IN EXPANDING LASER-PRODUCED PLASMAS

Intensity of the FWM signal

Let us consider the process of coherent FWM in a medium with a third-order non-linearity. We assume that the frequencies ω_1 , ω_2 , and ω_3 of the pumping waves are chosen in such a manner that the frequency of the FWM signal $\omega_{\text{FWM}} = \omega_1 + \omega_2 - \omega_3$ is close to the frequency of a certain atomic or ionic transition. The efficiency of this process is determined by the cubic non-linear optical susceptibility of the medium $\chi^{(3)} = \chi^{(3)}(\omega_{\text{FWM}}; \omega_1, \omega_2, -\omega_3)$. In what follows, we shall omit frequency arguments of the cubic susceptibility to simplify notations.

The power of the FWM signal produced in an extended non-linear medium irradiated with three laser beams with frequencies ω_1 , ω_2 and ω_3 , powers P_1 , P_2 and P_3 and wavevectors k_1 , k_2 and k_3 is given by^{33–36}

$$P_{\text{FWM}} \propto |\chi_r^{(3)} + \chi_{\text{nr}}^{(3)}|^2 P_1 P_2 P_3 G \quad (1)$$

where G is the phase-matching factor, $\chi_r^{(3)}$ is the resonant part of the cubic non-linear optical susceptibility of the medium and $\chi_{\text{nr}}^{(3)}$ is the non-resonant part of the cubic non-linear optical susceptibility, which generally includes the quasi-resonant component¹⁵ due to close resonances of plasma species and transitions in the continuous spectrum. For focused pumping beams with Gaussian spatial profiles, the phase-matching factor G can be written as^{33–36}

$$G = 2\pi \int_0^\infty |I|^2 r dr \quad (2)$$

$$I = \exp(-\kappa_1 L) \int_{-\zeta}^{\xi} d\xi' \frac{\exp[i(\Delta k - \kappa + \kappa_1)(\xi - \xi')(b/2)]}{(1 + i\xi')(a - i\xi')H} \times \exp(-r^2/H) \quad (3)$$

where $\Delta k = k_4 - k'$, k_4 is the wavevector of FWM radiation in the non-linear medium, $k' = k_1 + k_2 - k_3$, κ and κ_1 are the imaginary parts of the wavevectors k_4 and $k' = k_1 + k_2 + k_3$, respectively, $a = k''/k'$, $b = 2\pi a_{0i}^2 n(\lambda_i)/\lambda_i$ is the confocal parameter ($i = 1, 2$ and 3), a_{0i} is the waist radius of a Gaussian beam with the wavelength λ_i , L is the length of the non-linear medium, $\xi = 2(L - f)/b$ and $-\zeta = -2f/b$ are the boundaries of the non-linear medium written in terms of dimensionless coordinates, f is the coordinate of the center of waists of the pumping Gaussian beams and

$$H = \frac{1 + \xi^2}{a - i\xi'} + i(\xi - \xi') \quad (4)$$

The resonant part of the non-linear optical cubic susceptibility is proportional to the difference of populations N_1 and N_2 in the lower and upper atomic (or ionic) states involved in the resonant transition:

$$\chi_r^{(3)} = (N_1 - N_2) \bar{\chi}_r^{(3)} \quad (5)$$

where $\bar{\chi}_r^{(3)}$ is the resonant cubic non-linear optical susceptibility per single atom (or ion).

In an expanding plasma, the populations N_1 and N_2 of resonant levels are functions of time. Therefore, the overall non-linear optical susceptibility $\chi_r^{(3)}$ is also a function of time. Conceptually, time-dependent frequency-domain non-linear optical susceptibilities (defined as Fourier transforms of time-domain non-linear optical susceptibilities) can be consistently introduced only when both $\chi_r^{(3)}$ and $\chi_{\text{nr}}^{(3)}$ vary on a time-scale much greater than the durations of optical cycles of the light fields involved in the process. In the case of such a hierarchy of time-scales, we deal with a problem of non-linear spectrochronography,³⁷ when the properties of non-linear optical susceptibilities have to be determined not only in the frequency, but also in the time domain.

As can be seen from Eqns (1)–(5), the information concerning the kinetics and spatial distribution of the resonant species provided by temporal and spatial dependences of

the FWM signal is distorted by phase mismatch, absorption and interference of resonant and non-resonant parts of the cubic susceptibility. When the combination of frequencies $\omega_1 + \omega_2 - \omega_3$ is tuned into a resonance with the frequency of a transition between electronic states of an atom or an ion, one can expect a resonant enhancement of the susceptibility $\chi^{(3)}$ if this transition is simultaneously three- and one-photon allowed in the dipole approximation (we call such a situation a hyper-Raman resonance³⁸). However, because of the increase in one-photon absorption at the frequency ω_{FWM} and variation in phase-matching conditions, such enhancement of the cubic susceptibility does not necessarily increase the efficiency of frequency conversion through four-wave mixing. Moreover, conditions of the interference of resonant and non-resonant parts of the cubic susceptibility change in time, since time dependences of these quantities may differ from each other. This effect may also have a considerable influence on the behavior of the FWM signal in the time domain. However, in calculations of time dependences of the FWM signal, we shall assume that the non-resonant part of the cubic susceptibility is negligibly small compared with the resonant component at the maximum of a resonant line. This can be done (in contrast to spectral dependences, when additional measurements have to be performed, e.g. with the use of coherent ellipsometry, to separate resonant and non-resonant components of the cubic susceptibility¹⁵) around the maxima of sufficiently strong atomic or ionic resonances.¹² Generally, calculation of all the quantities involved in Eqns (1)–(3) is a complex problem. Analysis of this problem in the case of laser-produced plasma requires certain physical assumptions concerning plasma kinetics. A model of an expanding laser-produced plasma is described in the following section.

Plasma kinetics

The time variable is introduced into Eqns (1)–(5) through the model of plasma expansion. We employ a simple model of an expanding plasma based on the theory of point explosion.^{39–41} Within the framework of this approximation, the time dependence of the total concentration of plasma species is written as

$$n = n_0 \left(\frac{t_0}{t} \right)^{1.2} \quad (6)$$

where n_0 is the total plasma density at time t_0 .

For an adiabatic expansion of a plasma plume, the time dependence of plasma temperature is

$$T = T_0 \left(\frac{t_0}{t} \right)^{1.2(\gamma-1)} \quad (7)$$

where T_0 is the plasma temperature at time t_0 and γ is the adiabatic exponent.

Such an approach implies that the temperature is assumed to be common for all plasma components. This assumption seems adequate for our experimental conditions when FWM is employed to probe laser-produced plasmas at large delay times with respect to the moment of plasma creation.

Since the experiments on the FWM plasma spectroscopy have been carried out at atmospheric pressure of ambient air, we also assume that the laser-produced plasma consists of atoms and ions of nitrogen and oxygen, as well as atoms and ions of the target material. The composition of the laser-produced plasma is assumed to be governed by the Saha–Boltzmann equations:⁴²

$$\frac{N_e N_\alpha^Z}{N_\alpha^{Z-1}} = K = \frac{2S_\alpha^Z}{S_\alpha^{Z-1}} \left[\frac{2\pi m_e T}{h^2} \right]^{3/2} \exp \left(-\frac{E_\alpha^Z - \Delta E_\alpha^Z}{T} \right) \quad (8)$$

where m_e is the electron mass, h is Planck's constant, T is the plasma temperature, N_e is the electron concentration, E_α is the ionization potential, N_α^Z is the concentration of ions of sort α with a charge Z ,

$$\Delta E_\alpha^Z = \frac{Ze^2}{\lambda_{d\alpha}} \quad (9)$$

(where $\lambda_{d\alpha}$ is the Debye radius and e is the electron charge) is the reduction of the ionization potential due to Debye screening and S_α^Z is the partition function for ions of sort α with a charge Z :

$$S_\alpha^Z = \sum_k g_{\alpha k}^Z \exp \left(-\frac{E_{\alpha k}^Z}{T} \right) \quad (10)$$

where $g_{\alpha k}$ is the statistical weight of the k th state of sort α particles and $E_{\alpha k}$ is the energy of the k th state of sort α particles. In calculating partition functions, we assumed that the ionization potential in plasmas is reduced due to Debye screening by ΔE_α^Z .

For the computation of the concentrations of electrons, ions and atoms, the Saha equation [Eqn (8)] was supplemented with the conditions of electric neutrality:

$$N_e = \sum_\alpha Z N_\alpha^Z \quad (11)$$

the conservation of the number of particles:

$$n = \sum_{\alpha, Z} N_\alpha^Z \quad (12)$$

and the conservation of partial pressures:

$$\frac{1}{n} \sum_Z N_\alpha^Z = p_\alpha^0 \quad (13)$$

where p_α^0 is the initial content of plasma component α .

Solving the set of Eqns (6)–(13) and assuming that the plasma resides in the equilibrium state, we can find the population of the k th level with an energy $E_{\alpha k}$ for species of sort α in accordance with the Boltzmann equation:

$$N_{\alpha k}^Z = N_\alpha^Z \frac{g_{\alpha k}^Z}{S_\alpha^Z} \exp \left(-\frac{E_{\alpha k}^Z}{T} \right) \quad (14)$$

Radiative transitions have also been taken into account in more detailed simulations⁴ using the modified diffusion approximation,⁴³ which demonstrated that, in the case under study, these transitions have virtually no influence on the kinetics of the considered resonant atomic levels. Thus, the model described by Eqns (6)–(14) allows us to

compute the populations of all the atomic and ionic levels contributing to the FWM signal and to find the concentrations of the plasma species determining absorption and phase mismatch in the plasma.

Phase mismatch and absorption

With plasma composition and the distribution of plasma species in energy levels determined with the use of the model described in the previous section, we can calculate optical parameters of a laser-produced plasma that influence the intensity of the hyper-Raman resonant FWM signal, viz. phase mismatch and absorption coefficients at the relevant frequencies. In studying phase-mismatch effects in FWM, we should take into account the influence of both dispersion of resonant atoms and ions and the non-resonant contribution due to plasma electrons:

$$\Delta k = \Delta k_{r0} \frac{g_2 N_1 - g_1 N_2}{g_2 N_{10} - g_1 N_{20}} + \frac{\omega_p^2}{2c} \left(\frac{1}{\omega_1} + \frac{1}{\omega_2} - \frac{1}{\omega_3} - \frac{1}{\omega_{\text{FWM}}} \right) + \Delta k_0 \frac{n}{n_0} \quad (15)$$

where g_1 and g_2 are the statistical weights of the levels 1 and 2, respectively, N_{10} and N_{20} are the maximum populations of resonant levels 1 and 2, respectively, c is the speed of light in vacuum, Δk_{r0} is the maximum resonant contribution to the phase mismatch, corresponding to the maximum value of the difference $g_2 N_1 - g_1 N_2$, $\omega_p = \sqrt{4\pi N_e e^2 / m_e}$ is the plasma frequency and $\Delta k_0 n / n_0$ is the non-resonant component of the phase mismatch. Near the maximum of a hyper-Raman resonance, the quantity Δk_{r0} , which is written in the case of a Lorentzian line as $\Delta k_{r0} = (\delta \kappa_{r0} / (\delta^2 + 1))$ [$\delta = (\omega_{21} - \omega_{\text{FWM}}) / \nu$] is the frequency detuning of the FWM signal from the central resonance frequency ω_{21} normalized to the line half-width ν], is small, and the first term in Eqn (15) becomes negligible compared with the second and third terms.

For a light wave whose frequency is resonant to a one-photon transition (the FWM wave in the case of hyper-Raman resonances), the absorption coefficient can be written as

$$\kappa_r = \kappa_{r0} \frac{g_2 N_1 - g_1 N_2}{g_2 N_{10} - g_1 N_{20}} \quad (16)$$

Here, the maximum absorption coefficient is given by

$$\kappa_{r0} = \frac{2e^2 \pi f_r}{m_e c \nu} \left(N_{10} - \frac{g_1}{g_2} N_{20} \right) \quad (17)$$

where f_r is the relevant oscillator strength.

The coefficient of non-resonant absorption due to electron-ion collisions for the i th light wave involved in FWM ($i = 1, 2, 3$) can be written as

$$2\kappa_i = \frac{\omega_p^2 \gamma_{ei}}{\omega_i^2 c} \quad (18)$$

where γ_{ei} is the frequency of electron-ion collisions.

Qualitatively, the distortion of the information on the spatial distribution of atoms or ions in a plasma due

to phase matching and absorption effect can be understood in terms of characteristic lengths of a non-linear optical interaction in a medium: the length of phase matching $l_{\text{coh}} = \pi / (2|\Delta k|)$, absorption lengths $l_i = 1/\kappa_i$, and $l_{\text{FWM}} = 1/\kappa_r$, the interaction length l_{int} (which is determined by the geometry of FWM) and the length l_s that the FWM signal travels from the initial point of the interaction region to the exit of the medium (l_s will be estimated with its upper bound, the length of the medium L). FWM maps provide undistorted information on the spatial distribution of atoms or ions in a plasma when P_{FWM} scales as N^2 , which implies that the conditions

$$l_{\text{int}} < l_{\text{coh}}, l_1, l_2, l_3 \quad (19a)$$

and

$$L < l_{\text{FWM}} \quad (19b)$$

should be satisfied.

Since the characteristic lengths introduced above are functions of plasma parameters, we have to analyze how plasma parameters evolve in the process of plasma expansion and how the dynamics of plasma parameters influence the dependence of P_{FWM} on N . Such an analysis is provided in the following section.

Time evolution of plasma parameters

Numerical simulations were carried out for a plasma produced by laser radiation focused on a lead target. It was assumed that the frequency combination $\omega_1 + \omega_2 - \omega_3$ was tuned to the frequency of the transition between the $7s \ ^3P_0^o$ and $6p^2 \ ^3P_1$ states in Pb atoms (Fig. 1). To specify the fitting parameters involved in the model of a plasma described above, including the initial temperature T_0 , the initial density n_0 , parameter Δk_0 and the time-scale t_0 , we measured the transmission of a laser-produced plasma for all the light waves involved in the FWM process. Based on the results of these plasma-transmission measurements, we can neglect the influence of non-resonant absorption, described by κ_i , compared with absorption of the resonant wave with absorption coefficient κ_{r0} . We can also estimate the absolute value of the resonant absorption coefficient as $\kappa_{r0} \approx 1.4 \text{ cm}^{-1}$. With $n_0 = 10^{18} \text{ cm}^{-3}$, $T_0 = 0.73 \text{ eV}$, $t_0 = 400 \text{ ns}$ and $\Delta k_0 = 200 \text{ cm}^{-1}$ we were able to achieve reasonable agreement between the results of simulations and measurements simultaneously for transmission and FWM.

The time dependences of plasma temperature T , concentration n , electron density N_e , population difference $N_1 - N_2$ and the phase-matching factor G (for Gaussian

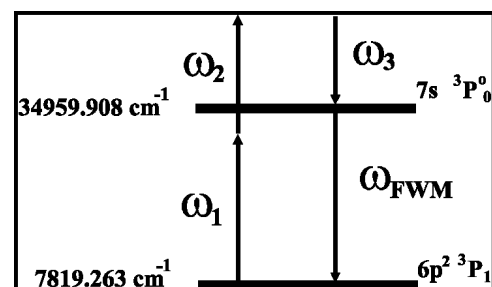


Figure 1. Diagram of a four-photon process with a hyper-Raman resonance involving excited states of a lead atom.

beams with a confocal parameter $b = 0.34$ cm focused at the center of a plasma with a length $L = 0.8$ cm) simulated with the use of the model described above are presented in Figs 2 and 3. As can be seen from the time dependence of the plasma temperature presented in Fig. 2, at least beginning with $\tau = t_0 = 400$ ns, the plasma temperature is always less than the difference in the energies of the resonant atomic states, which is approximately equal to 3.4 eV (Fig. 1). Therefore, the population of level 2 is much less than that of level 1, and the population difference $N_1 - N_2$ (curve 2 in Fig. 3) follows the population of level 1 (this conclusion also follows from the results of numerical simulations). At early stages of plasma expansion, the population of level 1 is small because a considerable fraction of atoms is excited into high-lying states or ionized. At these stages, the population of level 1 grows in the process of plasma expansion owing to recombination and the relaxation of excited states through this level. When the number of atoms coming to this level from higher lying state becomes less than the number of atoms outgoing from this level to lower states, N_1 begins to decrease. As a result, the population difference $N_1 - N_2$ increases at the initial stage of plasma expansion, reaches its maximum, and then decreases (Fig. 3).

The factor G displays an oscillatory behavior at the initial stage, which is characteristic of phase-matching effects,⁴⁴ and then grows owing to the decrease in the concentration of resonant atoms and plasma electrons (Fig. 3). Characteristic time-scales of variations of $N_1 - N_2$

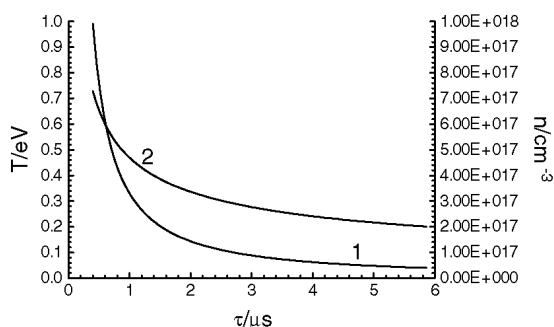


Figure 2. Kinetics of (1) plasma density n and (2) temperature T in an expanding laser-produced plasma.

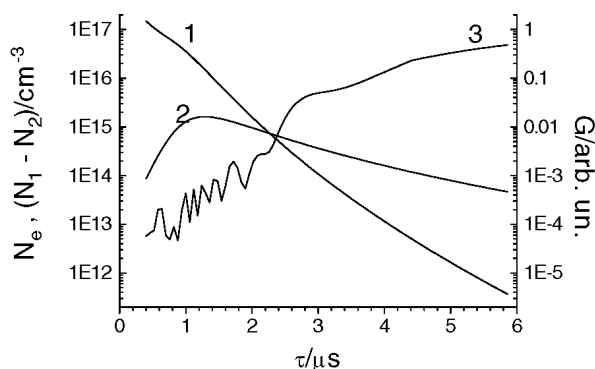


Figure 3. Time dependences of (1) the electron density N_e , (2) the population difference $N_1 - N_2$ and (3) the phase-matching factor G for Gaussian beams with a confocal parameter $b = 0.34$ cm focused at the center of a plasma with a length $L = 0.8$ cm.

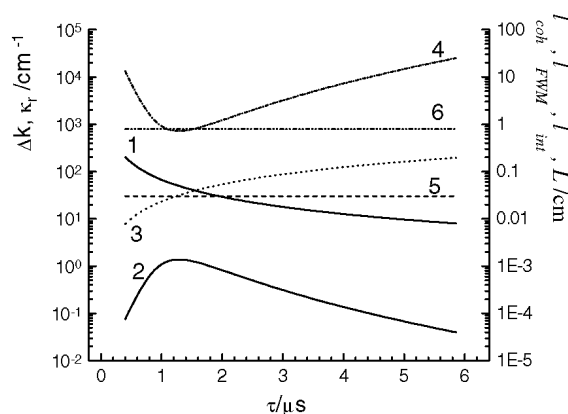


Figure 4. Time dependences of (1) the phase mismatch Δk , (2) resonant absorption coefficient κ_r , (3) coherence length l_{coh} , (4) absorption length of the FWM signal l_{FWM} , (5) the FWM interaction length l_{int} and (6) the length of the medium L for an expanding laser-produced plasma.

and G depend on the sort of atoms being probed and plasma parameters.

Figure 4 displays the behavior of the phase mismatch Δk (curve 1), resonant absorption coefficient κ_r (curve 2), and characteristic lengths l_{coh} (curve 3) and l_{FWM} (curve 4) in a plasma with the above-specified parameters. For comparison, the interaction length l_{int} for the implemented folded FWM scheme and the length of the medium L are shown by straight lines 5 and 6, respectively. Importantly, while l_1 , l_2 and l_3 remain much greater than the interaction length l_{int} of the implemented folded FWM scheme (straight line 5) within the entire range of delay times and the absorption length of the FWM signal l_{FWM} exceeds the length of the medium L (straight line 6) everywhere except for a narrow region around $\tau = 1.3$ μs , l_{coh} is less than the interaction length l_{int} for small delay times. With decrease in the concentration of resonant atoms and electrons in the process of plasma expansion and cooling, l_{coh} increases and becomes equal to l_{int} at $\tau \approx 1.2$ μs (the point where curve 3 intersects straight line 5 in Fig. 4). This prediction concerning the behavior of absorption and phase mismatch in a laser-produced plasma is consistent with the results of experimental measurements.¹² Thus, for sufficiently small τ , when $l_{\text{int}} < l_{\text{coh}}$ and/or $L \approx l_{\text{FWM}}$, the dependence of P_{FWM} on the concentration may deviate from N^2 . In such a situation, a procedure for determining the spatial distributions of excited atoms and ions in a plasma from FWM intensity maps becomes much more complicated, since it should be performed with allowance for the influence of phase mismatch and one-photon absorption. For $\tau > 2.0$ μs , conditions (19a) and (19b) are satisfied, P_{FWM} can be approximated with a quadratic function of N , and the maps of the FWM signal provide undistorted information on the spatial distribution of atoms or ions in a plasma.

EXPERIMENTAL

Experimental setup

The experimental setup for FWM imaging of spatial distribution of excited atoms and ions in a laser-produced plasma (Fig. 5) consisted of a probing laser system, a laser

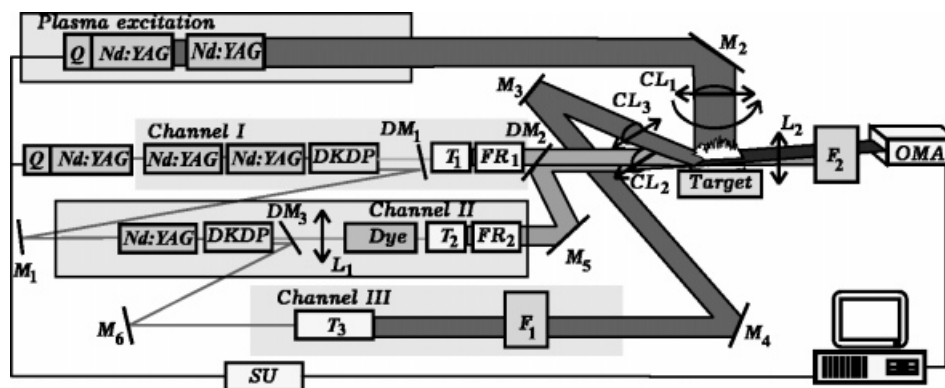


Figure 5. Experimental setup for the FWM imaging of a low-temperature laser-produced plasma: DM₁–DM₃, dichroic mirrors; FR₁ and FR₂, Fresnel rhombi; M₁–M₆, rotating mirrors; T₁–T₃, telescopes; F₁ and F₂, sets of optical filters; OMA, optical multi-channel analyzer; SU, synchronization unit; CL₁–CL₃, cylindrical lenses; and L₁ and L₂, lenses.

system for the generation of the plasma of optical breakdown, a synchronization unit and the detection system. The probing laser system (described in detail elsewhere¹²) was based on a Q-switched Nd:YAG master oscillator, which generated 15 ns laser pulses at the wavelength $\lambda_0 = 1.064 \mu\text{m}$. Amplified fundamental radiation was converted into the second harmonic in a CDA crystal. Second-harmonic radiation was used to pump a dye laser, which generated frequency-tunable radiation within the range $\lambda_2 = 0.560\text{--}0.600 \mu\text{m}$ with an oscillation bandwidth of about 0.5 cm^{-1} . Since the main source of experimental errors was associated with fluctuations of plasma parameters from pulse to pulse, beam referencing,^{30,45} which compensated for intensity fluctuations along the profile of the dye-laser beam, did not permit us to improve noticeably the accuracy of measurements and, therefore, was not used in experiments involving averaging over several laser pulses. The polarization of radiation with the wavelength $\lambda_0 = 1.064 \mu\text{m}$ was fixed, whereas polarizations of the second harmonic and dye-laser radiation were varied by means of double Fresnel rhombs in order to ensure the best contrast of FWM spectra.

The system for plasma excitation employed a Q-switched Nd:YAG master oscillator, which produced 15 ns laser pulses with an energy of about 200 mJ.¹² A laser beam produced by this system was focused on the surface of a metal target with a 10 cm focal length cylindrical lens CL₁ (Fig. 5). By rotating this lens, we were able to vary the orientation of a laser-produced spark with respect to the incident beams and perform plasma probing in different directions. An electric timing unit was designed to synchronize plasma-excitation and plasma-probing laser pulses so that the plasma was irradiated with three-color pumping beams with a variable delay time τ with respect to plasma excitation. With different delay times τ , we were able to study linear and non-linear optical parameters of an ionized gas and to investigate changes in the regime of nonlinear-optical interaction at various stages of plasma expansion.

Second-harmonic and dye-laser beams focused with a 10 cm focal length cylindrical lens CL₂ formed broad light sheets with a width of 4 mm and a height of 20 μm in the beam-waist area. The beam of fundamental radiation was focused with an identical cylindrical lens CL₃, which formed a similar beam sheet making an angle α with the second harmonic and dye laser radiation in the beam-waist area (Fig. 5). The FWM signal generated in the

one-dimensional area formed by the intersection of a triad of incident beams was collimated with a spherical lens and detected with an optical multi-channel analyzer (with no intensifier) placed behind a set of bandpass filters. The one-dimensional FWM signal recorded with this analyzer was processed with a dedicated software and was stored in a PC.

FWM plasma imaging

The implemented experimental technique for imaging the relative populations of excited states of atoms in a decaying low-temperature plasma of optical breakdown induced on the surface of a metal target is based on three-color coherent FWM with hyper-Raman resonances, when the frequency of the FWM signal $\omega_{\text{FWM}} = \omega_1 + \omega_2 - \omega_3$ (where ω_3 is the frequency of fundamental radiation of an Nd:YAG laser, ω_1 is the frequency of the second harmonic of an Nd:YAG laser and ω_2 is the frequency of a tunable dye laser) is resonant to some atomic (or ionic) transition in a laser-produced plasma (Fig. 1). The one-dimensional FWM signal generated in a folded FWM scheme^{16,32} [Fig. 6(a)] is employed to image the spatial

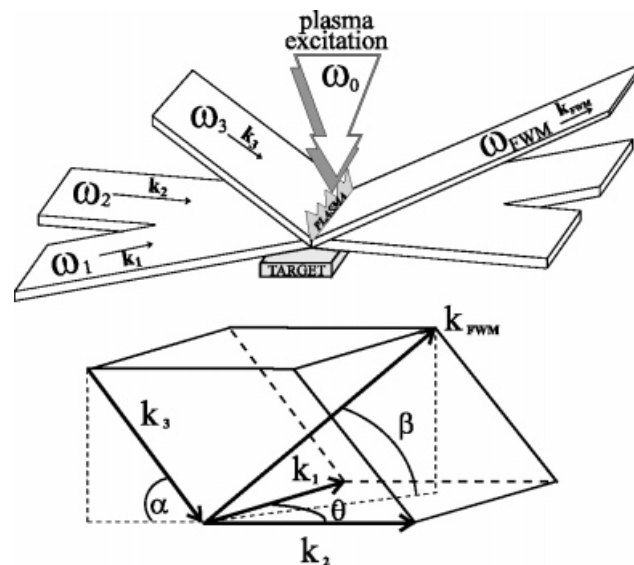


Figure 6. One-dimensional imaging of atoms in a laser-produced plasma by means of coherent FWM in broad beams: (a) diagram of light beams and (b) diagram of wavevectors.

distributions of plasma atoms line by line. In this scheme, a pair of cylindrically focused coplanar broad light beams with frequencies $\omega_1 = 2\omega_3$ and ω_2 and wavevectors \mathbf{k}_1 and \mathbf{k}_2 , forming a small angle θ , irradiate a thin plasma layer in a plane parallel to the plane of the target. A cylindrically focused beam with frequency ω_3 and wavevector \mathbf{k}_3 , which makes an angle α with the plane of the \mathbf{k}_1 and \mathbf{k}_2 vectors, irradiates the laser-produced spark from above. The FWM signal is generated in the direction \mathbf{k}_{FWM} determined by phase-matching conditions, forming an angle β with the plane of the target [Fig. 6(a) and 6(b)]. By imaging the one-dimensional FWM signal onto a CCD array, we were able to map the spatial distribution of resonant particles in the plasma line by line.

Absorption measurements

Light beams propagating in laser-produced plasmas may experience resonant and non-resonant absorption due to atomic/ionic and electronic plasma components, respectively. Such processes eventually lower the intensity of the FWM signal and should be taken into account in the reconstruction of the maps of spatial distributions of plasma species from the maps of the FWM signal. To assess the influence of one-photon absorption at different stages of plasma expansion, we measured plasma transmission for all the probing beams and a beam at the frequency of the FWM signal as functions of the delay time τ . All the light beams in these experiments were focused with a spherical lens with a focal length of 15 cm. For the pumping waves, absorption remained negligible (less than 5% for $\tau > 100$ ns). To measure plasma transmission at the frequency of the FWM signal, we mixed fundamental frequency ω_0 with the dye-laser frequency ω_2 in a KDP crystal. Such a wave-mixing process yielded a signal at the frequency $\omega_{\text{WM}} = \omega_2 + \omega_3 = \omega_1 + \omega_2 - \omega_3 = \omega_{\text{FWM}}$ (since $\omega_1 = 2\omega_3$). The normalized plasma transmission coefficient at the frequency of the FWM signal as a function of τ is presented in Fig. 7. As can be seen from this figure, plasma transmission at the frequency of the FWM signal reaches its minimum at $\tau \approx 1.3$ μs , when more than 90% of FWM signal can be absorbed. The information concerning one-photon absorption in laser-produced plasmas was employed to specify the fitting parameters involved in the model of a plasma described above, including the initial temperature T_0 , the initial plasma density n_0 , parameter Δk_0 and the time-scale t_0 . Setting, in accordance with the experimental results, $\kappa_{r0} \approx 1.4$ cm^{-1} , $n_0 = 10^{18}$ cm^{-3} ,

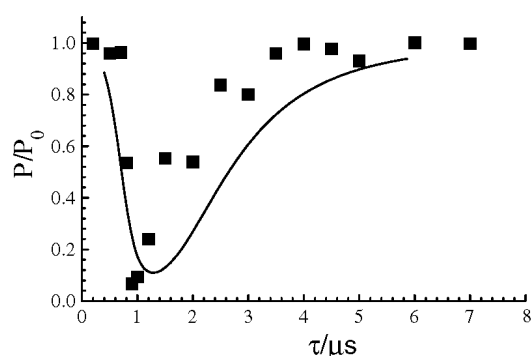


Figure 7. The normalized plasma transmission coefficient at the frequency of the FWM signal as a function of the delay time τ : dots, experimental data; solid curve, results of simulations.

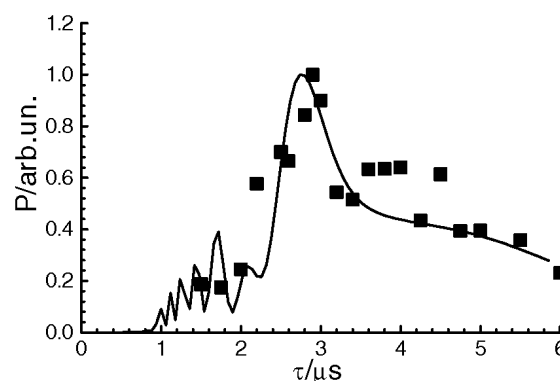


Figure 8. The FWM signal from a laser-produced plasma as a function of the delay time τ : dots, experimental data; solid curve, results of simulations. Experiments were performed with collinear laser beams focused with a 15 cm focal length spherical lens.

$T_0 = 0.73$ eV, $t_0 = 400$ ns and $\Delta k_0 = 200$ cm^{-1} and neglecting, based on the experimental data, the influence of non-resonant absorption, described by κ_i , as compared with absorption of the resonant wave with absorption coefficient κ_{r0} , we were able to reproduce simultaneously with reasonable accuracy the results of transmission and FWM experiments performed with collinear laser beams focused with a 15 cm focal length spherical lens (Figs 7 and 8).

RESULTS AND DISCUSSION

One-dimensional FWM imaging of Pb atoms

For the experimental investigation of the spatial distribution of the populations in excited states of atoms in the plasma of optical breakdown, we employed a four-photon scheme $\omega_{\text{FWM}} = \omega_1 + \omega_2 - \omega_3$, where ω_3 is the frequency of fundamental radiation of an Nd:YAG laser ω_1 is the frequency of the second harmonic of an Nd:YAG laser and ω_2 is the frequency of a tunable dye laser. The frequency of the dye laser was chosen in such a manner as to ensure a resonance between the frequency ω_{FWM} of the FWM signal and the frequency of the probed transition between electronic states of atoms excited in a laser-produced plasma. In our experiments, the frequency combination $\omega_1 + \omega_2 - \omega_3$ was tuned to the frequency of the transition between the $7s$ $^3P_0^0$ and $6p^2$ 3P_1 states in Pb atoms (Fig. 1). Under these conditions, we observed a resonant enhancement of the FWM signal at the wavelength $\lambda_{\text{FWM}} = 368.45$ nm due to a hyper-Raman resonance. The dependence of the FWM signal intensity on the delay time between the laser pulses of three-color pumping and the laser pulse used for plasma excitation provides the information concerning the depopulation kinetics of the above-specified atomic states. Studying the intensity of the FWM signal as a function of spatial coordinates, we were able to extract the information concerning the spatial distribution of excited Pb atoms.

The 2-D maps shown in Figs 9 and 10 were obtained with $\theta = 0$ and $\alpha \approx 3^\circ$ in the longitudinal (see the top of Fig. 9) and transverse (see the top of Fig. 10) schemes of plasma imaging. The employed technique of plasma

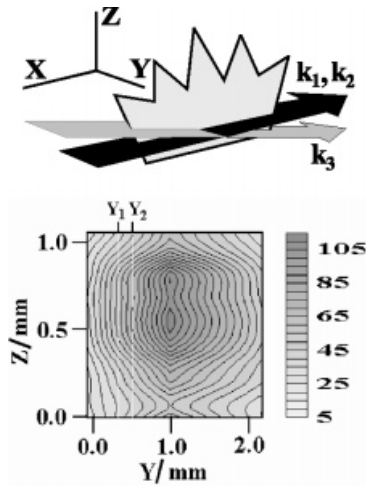


Figure 9. Line-by-line plasma imaging using one-dimensional FWM in the longitudinal direction: top, the scheme of longitudinal imaging; bottom, two-dimensional maps of the FWM signal power with a resonance due to Pb atomic transitions in a laser-produced plasma. The vertical lines show the slice y_1 – y_2 mapped in Fig. 10.

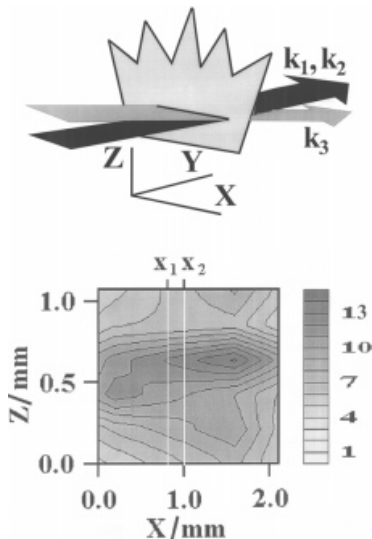


Figure 10. Line-by-line plasma imaging using one-dimensional FWM in the transverse direction: top, the scheme of transverse imaging; bottom, two-dimensional maps of the FWM signal power with a resonance due to Pb atomic transitions in a laser-produced plasma. The vertical lines show the slice x_1 – x_2 mapped in Fig. 9.

imaging provides information concerning the spatial distribution of plasma species along the line corresponding to the intersection of the light beams with wavevectors \mathbf{k}_1 , \mathbf{k}_2 and \mathbf{k}_3 [see Figs 6(a) and 6(b)]. However, to compose a 2-D image of some plasma area, we have to detect a considerable number of one-dimensional FWM signals, which means that averaging should be performed to smooth out fluctuations in plasma parameters from pulse to pulse. To generate 2-D maps of spatial distributions, we detected hyper-Raman resonant one-dimensional FWM signals line by line by scanning the laser-produced spark with a step of 50 μm along the z -axis. Thus, 21 images of one-dimensional FWM were used to generate the 2-D maps shown in Figs 9 and 10. Each line in these maps represents the result of averaging over 100 laser

pulses. Interpolating the results of FWM measurements with the use of a standard built-in computer procedure and representing the distribution of the FWM intensity thus obtained by levels of gray scale in a 2-D map, we were able to visualize the spatial distribution of the relative populations of the relevant atomic states.

It should be noted that, since the FWM signal intensity is a non-linear (quadratic) function of the density of resonant species, averaging over different measurements, which has to be done to smooth out jumps in the FWM intensity from pulse to pulse, gives rise to systematic deviations of FWM images from real spatial distributions of the density of resonant species. In other words, the averaged FWM intensity generally converges to a value other than the square of the mean density of species to be measured. Fluctuations of the intensities of laser beams involved in FWM is another source of errors when the information concerning the spatial distribution of atoms or ions in a plasma has to be extracted from two-dimensional FWM images. In our experiments, fluctuations of the laser powers ($\sigma_1/\langle P_1P_2P_3 \rangle \leq 0.15$, where σ_1^2 is the variance of the product of laser powers $P_1P_2P_3$) remained much less than the fluctuations of the total signal ($\sigma_{\text{FWM}}/\langle P_{\text{FWM}} \rangle \approx 0.40$, where σ_{FWM}^2 is the variance of the FWM signal power), which implies that the relative fluctuations of laser powers are small as compared with relative fluctuations of the cubic susceptibility (i.e. fluctuations of plasma parameters), and the distortions in FWM images in our experiments were mainly due to the fluctuations of plasma parameters. To provide quantitative estimates of experimental errors arising due to this factor, we employ Eqns (1) and (5) and assume that the non-resonant part of the cubic susceptibility is small as compared with the resonant component to derive the following relation between the mean difference of populations in resonant excited states, $\langle N \rangle$, and measurable statistical characteristics of the FWM signal:

$$\langle N \rangle \approx \frac{\sqrt{\langle P_{\text{FWM}} \rangle}}{\bar{\chi}_r^{(3)} \sqrt{b}} \left(1 - \frac{\sigma_{\text{FWM}}^2}{8 \langle P_{\text{FWM}} \rangle^2} \right) \quad (20)$$

where b is a constant and angle brackets denote averaging. Thus, owing to the non-linear dependence of the FWM signal on the density of resonant species, coherent FWM, in accordance with Eqn (20), gives an overestimated value of the density of resonant species. However, for our experiments, with $\sigma_{\text{FWM}}^2/\langle P_{\text{FWM}} \rangle^2 \approx 0.16$, the deviation of the map of the concentration of resonant particles from the map of the FWM signal was small (about 2%).

Although distortions in the maps of the FWM signal due to one-photon absorption and phase mismatch can be corrected with an appropriate processing procedure, optimal conditions for FWM plasma imaging are clearly achieved when FWM plasma images cease to be distorted due to absorption and phase-matching effects, i.e. when inequalities (19a) and (19b) are met. As was shown above, conditions (19a) are satisfied to the right of the point where curve 3 in Fig. 4, representing l_{coh} , intersects straight line 5, which corresponds to the interaction length l_{int} . Condition (19b) is met everywhere except for a small range of delay times around 1.3 μs , where absorption of the FWM signal reaches its maximum. Thus, the maps of the FWM signal presented in Figs 9 and 10, which were generated line by line for $\tau = 3.0 \mu\text{s}$, represent the maps

of the spatial distributions of Pb atoms in a laser-produced plasma.

Averaged density profiles of Pb atoms measured by means of one-dimensional FWM correlated fairly well with the averaged results of point-by-point FWM measurements.^{11,12} In addition, performing FWM measurements in a gas cell uniformly filled with CO₂ gas, we obtained nearly uniform (within the limits of experimental errors) maps of one-dimensional FWM signal, confirming that the experimental uncertainty of FWM imaging in that case was restricted to experimental errors resulting from fluctuations of laser powers. Generally, the adequacy of coherent hyper-Raman resonant FWM as a method to measure spatial distributions of atoms and ions in plasmas has been earlier demonstrated in experiments with electric-discharge plasmas,⁴⁶ where the density profiles of copper and bromine atoms measured with the use of the point-by-point FWM technique agreed well with the results obtained by means of absorption and emission spectroscopy.

Sensitivity of one-dimensional FWM plasma imaging

One of the crucial issues that eventually determines whether it is expedient to apply a folded FWM scheme in broad beams for plasma diagnostics is the possibility to achieve a reasonable compromise between the intensity of the FWM signal, on the one hand, and the area of FWM probing, on the other hand. To put it differently, the atomic or ionic transition to be probed should be intense enough to allow the probing of a sufficiently large area with a reasonably high accuracy in the direction of imaging. The intensity of the FWM signal in the considered experimental scheme depends on the relevant cubic non-linear optical susceptibility per single atoms $\bar{\chi}_r^{(3)}$, the population difference $N_1 - N_2$ and the phase-matching factor G [see Eqns (1)–(5)]. The evolution of the last two quantities in the process of plasma expansion, which is presented in Fig. 3, has been discussed above. A characteristic time dependence of the FWM signal observed in experiments with Pb atoms is shown by dots in Fig. 8. The solid line represents the results of numerical simulations, which fit experimental data reasonably well, thus confirming the adequacy of the employed plasma model.

Comparison of Figs 3, 4 and 8 shows that phase-mismatch and absorption effects may play an important role at early stages of plasma expansion, complicating the interpretation of FWM measurements. In particular, as can be seen from Figs 3 and 4, the maps of the FWM signal obtained with delay times $\tau < 2 \mu\text{s}$ should be corrected for phase mismatch and absorption in accordance with Eqns (1)–(5). Luckily for the sensitivity of imaging of lead atoms, the FWM signal reaches its maximum (Fig. 8) at delay times when the coherence length l_{int} (curve 3 in Fig. 4) is greater than the length of interaction (curve 5 in Fig. 4), and the absorption length of the FWM signal (curve 4 in Fig. 4) exceeds both the length of the medium (curve 6 in Fig. 4) and the interaction length. Two-dimensional maps presented in Figs 9 and 10 were generated with line-by-line FWM imaging for a delay time $\tau \approx 3.0 \mu\text{s}$, which corresponded to the maximum of the FWM signal, when N_1 was about $3 \times 10^{14} \text{ cm}^{-3}$. With the signal-to-noise ratio being of the order of 10^3 , we

find that the sensitivity of one-dimensional imaging of Pb atoms in the considered experimental scheme can be estimated as $3 \times 10^{13} \text{ cm}^{-3}$. Since the main source of noise in such experiments is associated with plasma emission, the sensitivity of FWM imaging technique can be further improved with a careful spatial and temporal filtering of the FWM signal.

Spatial resolution

In three-color folded FWM imaging, the FWM signal remains unresolved along the direction of imaging (along the wavevector \mathbf{k}_{FWM}) within the interaction length l_{int} , while the spatial resolution in the direction perpendicular to the wavevector \mathbf{k}_{FWM} is determined by the resolution of the imaging system. Since a spherical lens with a large aperture (2.5 cm) was used in our experiments to collimate the FWM beam, the spatial resolution along the imaged line was mainly limited by the size of a pixel of the CCD camera (15 μm) rather than by diffraction effects.

The spatial resolution of FWM imaging along two orthogonal directions can be conveniently characterized in terms of parameters invariant with respect to the angle β (Fig. 11), which is determined by the dispersion of the medium. In particular, the spatial resolution of the implemented three-color folded FWM technique can be characterized by the sizes R_1 and R_2 of the intersection area of the probing beams (Fig. 11). The parameters R_1 and R_2 can be understood as the sizes of a plasma volume contributing to the one-dimensional FWM signal or, in other words, to each line in an FWM plasma image. These parameters can be expressed in terms of the waist sizes w_1 , w_2 and w_3 of the pumping beams with wavevectors \mathbf{k}_1 , \mathbf{k}_2 and \mathbf{k}_3 , respectively, and the angle α in the following manner:

$$R_1 = \frac{w_3 + w_{12} \cos \alpha}{\sin \alpha} \quad (21)$$

$$R_2 = w_{12} \quad (22)$$

where $w_{12} = (w_1^{-2} + w_2^{-2})^{-1/2}$ (θ was set equal to zero).

The interaction length in this case can be estimated as

$$l_{\text{int}} = \frac{w_3}{\sin(\alpha + \beta)} \quad (23)$$

For the geometry of FWM introduced above, we have $w_1 = w_2 = w_3 = 20 \mu\text{m}$, $\alpha \approx 3^\circ$ and $\beta \approx 1^\circ$ and Eqns (21)–(23) yield the following estimates: $l_{\text{int}} \approx 300 \mu\text{m}$, $R_1 \approx 680 \mu\text{m}$ and $R_2 \approx 14 \mu\text{m}$.

Thus, each line in one-dimensional FWM implemented in our experiments corresponds to a signal collected from

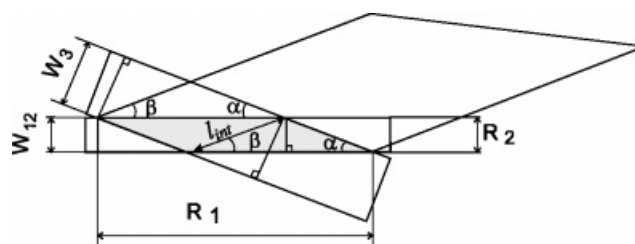


Figure 11. Spatial resolution of 1-D FWM plasma imaging.

a $680 \times 14 \mu\text{m}$ plasma element, providing an opportunity to resolve plasma elements with such dimensions. Obviously, the spatial resolution of the FWM technique is achieved at the expense of the intensity of the FWM signal, which is proportional in the phase-matched regime in the absence of absorption to $(I_{\text{int}})^2$. We should note also that it is due to the small interaction length that we are able to implement phase-matched FWM and to obtain images of the spatial distribution of atoms in a laser-produced plasma free of distortions due to phase mismatch.

CONCLUSION

One-dimensional coherent FWM with hyper-Raman resonances allows line-by-line imaging of the atomic distribution of excited atoms in a low-temperature plasma of optical breakdown. The experimental technique presented in this paper implies that a pair of cylindrically focused coplanar broad light beams forming a small angle irradiate a thin plasma layer in a plane parallel to the plane of the target. The third cylindrically focused light beam irradiates the laser-produced spark from above. The FWM signal is generated in the direction of phase matching. Imaging the interaction region on to a CCD array in FWM light yields single-pulse maps of the spatial distribution of resonant particles in the plasma. The developed scheme was applied to map excited lead atoms in a low-temperature laser-produced plasma.

It is demonstrated that effects of phase mismatch and one-photon absorption may considerably complicate the interpretation of the maps of the FWM signal. Comparison of the measured time dependences of plasma parameters with the results of numerical simulations of plasma expansion allowed us to estimate directly the influence of phase mismatch and one-photon absorption on the regime of non-linear optical interaction in a laser-produced plasma. Experimental conditions when resonant and non-resonant FWM interactions occur in the regime close to phase matching and where the influence of one-photon absorption is negligible were determined. In this regime, we mapped the spatial distribution of lead atoms in a laser-produced plasma using one-dimensional hyper-Raman FWM.

The basic advantage of the proposed approach is that it provides an opportunity to generate plasma maps line by line, which considerably reduces the number of measurements and improves the reliability of plasma analysis as compared with point-by-point imaging. Such a procedure holds much promise for the investigation of spatially inhomogeneous fast processes in a multi-component laser-produced plasma.

Acknowledgments

The research described in this paper was made possible in part by Award No. RPI-255 of the US Civilian Research and Development Foundation for the Independent States of the Former Soviet Union (CRDF). This study was also partially supported by INTAS project No. 97-0369.

REFERENCES

- Bloembergen N. *Nonlinear Optics*. Benjamin: New York, 1965.
- Druet S, Taran J-P. *Prog. Quantum Electron.* 1981; **7**: 1.
- Akhmanov SA, Koroteev NI. *Methods of Nonlinear Optics in Spectroscopy of Light Scattering*. Nauka: Moscow, 1981.
- Gladkov SM, Zheltikov AM, Koroteev NI, Koleva IS, Fedotov AB. *Sov. Tech. Phys. Lett.* 1989; **15**: 505.
- Fedotov AB, Gladkov SM, Koroteev NI, Zheltikov AM. *J. Opt. Soc. Am. B* 1991; **8**: 373; Rebane AK, Krylov VN, Koroteev NI, Zheltikov AM. *Quantum Electron.* 1996; **26**: 283; Fedotov AB, Koroteev NI, Loy MMT, Xiao X, Zheltikov AM. *Opt. Commun.* 1997; **133**: 587.
- Kubodera S, Nagata Y, Akiyama Y, Midorikawa K, Obara M, Tashiro H, Toyoda K. *Phys. Rev. A* 1993; **48**: 4576.
- Theobald W, Wulker C, Schafer FP, Chichkov BN. *Opt. Commun.* 1995; **120**: 177.
- Backus S, Peatross J, Zeek Z, Rundquist A, Taft G, Murnane MM, Kapteyn HC. *Opt. Lett.* 1996; **21**: 665.
- Miller JC (ed.). *Laser Ablation: Principles and Applications*. Springer Series in Materials Science, Vol. 28. Springer: Berlin, 1994.
- Chrisey DB, Hubler GK (eds). *Pulsed Laser Deposition of Thin Films*. Wiley: New York, 1994.
- Akimov DA, Fedotov AB, Koroteev NI, Naumov AN, Sidorov-Biryukov DA, Zheltikov AM. *Opt. Commun.* 1997; **140**: 259.
- Fedotov AB, Koroteev NI, Naumov AN, Sidorov-Biryukov DA, Zheltikov AM. *J. Nonlinear Opt. Phys. Mater.* 1997; **6**: 387.
- Gladkov SM, Zheltikov AM, Koroteev NI, Rychev MV, Fedotov AB. *Sov. J. Quantum Electron.* 1989; **19**: 923.
- Koroteev NI. *Sov. Phys. Usp.* 1987; **30**: 628.
- Koroteev NI, Naumov AN, Sidorov-Biryukov DA, Zheltikov AM. *Laser Phys.* 1997; **7**: 45.
- Akimov DA, Ewart P, Fedotov AB, Koroteev NI, Naumov AN, Sidorov-Biryukov DA, Zheltikov AM. *Laser Phys.* 1997; **7**: 755.
- Regnier PR, Taran JP-E. *Appl. Phys. Lett.* 1973; **23**: 240.
- Lapp M, Penney CM (eds). *Laser Raman Gas Diagnostics*. Plenum: New York, 1974.
- Eckbreth AC. *Laser Diagnostics for Combustion Temperature Species*, Abacus: Cambridge, MA, 1988.
- Murphy DV, Long MB, Chang RK, Eckbreth AC. *Opt. Lett.* 1979; **4**: 167.
- Snow JB, Zheng J, Chang RK. *Opt. Lett.* 1983; **8**: 599.
- Abrams RL, Lind RC. *Opt. Lett.* 1978; **2**: 94.
- Fisher RA. *Optical Phase Conjugation*. Academic press: London, 1983.
- Pender J, Hesselink L. *Opt. Lett.* 1985; **10**: 264.
- Ewart P, Ferguson AI, O'Leary SV. *Opt. Commun.* 1981; **40**: 147.
- Ewart P, O'Leary SV. *J. Phys. B* 1982; **15**: 3669.
- Ewart P, O'Leary SV. *Opt. Lett.* 1986; **11**: 279.
- Ewart P, Snowdon P, Magnusson I. *Opt. Lett.* 1989; **14**: 563.
- Rakestraw DJ, Farrow RL, Dreier T. *Opt. Lett.* 1990; **15**: 709.
- Ewart P, Smith PGR, Williams RB. *Appl. Opt.* 1997; **36**: 5959.
- Jonuscheit J, Thumann A, Schenk M, Seeger T, Leipertz A. *Opt. Lett.* 1996; **21**: 1532.
- Akimov DA, Fedotov AB, Koroteev NI, Miles RB, Naumov AN, Sidorov-Biryukov DA, Zheltikov AM. *Opt. Lett.* 1999; **24**: 478.
- Ward JF, New GHC. *Phys. Rev.* 1969; **185**: 57.
- Bjorklund GC. *IEEE J. Quantum Electron.* 1975; **QE-11**: 287.
- Reintjes JF. *Nonlinear Optical Parametric Processes in Liquids and Gases*. Academic press: Orlando, FL, 1984.
- Koroteev NI, Naumov AN, Zheltikov AM. *Laser Phys.* 1994; **4**: 1160.
- Koroteev NI. *Moscow Univ. Phys. Bull.* 1996; **51**(6): 1.
- Fedotov AB, Ilyasov OS, Koroteev NI, Zheltikov AM. *Nuovo Cimento D* 1992; **14**: 1003.
- Sedov LI. *Methods Similarity and Dimensions in Mechanics*, Nauka: Moscow, 1967.

40. Korobeinikov VP, Mel'nikova NS, Ryazanov EV. *Theory of Point Explosion*. Fizmatgiz: Moscow, 1961.
41. Ostrovskaya GV, Zaidel' AN. *Usp. Fiz. Nauk* 1973; **111**: 579.
42. Key MH, Hutcheon RJ. *Adv. At. Mol. Phys.* 1980; **16**: 201.
43. Biberman LM, Vorob'ev VS, Yakubov IT. *Kinetics of Nonequilibrium Low-Temperature Plasmas*. Nauka: Moscow, 1982.
44. Naumov AN, Koroteev NI, Zheltikov AM. *Laser Phys.* 1995; **5**: 965.
45. Antcliff RR, Jarrett O Jr. *Rev. Sci. Instrum.* 1987; **58**: 2075.
46. Zheltikov AM, Ilyasov OS, Isaev AA, Koroteev NI. *Bull. Russ. Acad. Sci., Phys.* 1992; **56**: 1170.